Ocean Modelling 204 (2026) 102814

Contents lists available at ScienceDirect

Ocean Modelling

journal homepage: www.elsevier.com/locate/ocemod

Ring assistance of tracer transport across the Kuroshio Extension: observation and simulation

M.A. Lebedeva [a,b,*], M.V. Budyansky [a,b], S.V. Prants [a], V.B. Lobanov [a], A.F. Sergeev [a], A.A. Udalov [a], A.A. Didov [a,b]

[a] V.I. Il'ichev Pacific Oceanological Institute, Far Eastern Branch, Russian Academy of Sciences, 43 Baltiyskaya St., Vladivostok, 690041, Russia
[b] St. Petersburg State University, St. Petersburg, 199034, Russia

ARTICLE INFO

Keywords:
Kuroshio Extension
Cross-jet transport
Fukushima tracers
Kuroshio rings
Simulation and ship observation

ABSTRACT

Tracking the spread of radionuclides following the accident at the Fukushima-Daiichi Nuclear Power Plant (FDNPP) in 2011 and since the start of controlled discharges of purified water in 2023 is important for assessing radiation risks and for understanding water mass transport in the confluence zone of the Kuroshio Extension (KE) and Oyashio currents. It is widely accepted that the powerful KE acts as a nearly impermeable barrier to cross-jet transport (CJT) of tracers. However, FDNPP-derived radiocesium was observed south of the KE front, raising the question of how such transport can occur. A 13-year particle-tracking simulation showed that virtual tracers released near the FDNPP site could cross the KE by moving southward along transport pathways, either due to shifts in the position of KE meanders or via Kuroshio rings. In both scenarios, tracers may end up on the southern side of the KE. CJT occurs when groups of tracers coherently cross the jet over a short period, taking advantage of transient transport corridors. In 2024, virtual FDNPP tracers were identified inside two cyclonic rings south of the KE. Observations from a cruise in June 2024 confirmed that these rings contained core water of subarctic origin. This finding was further supported by altimetry-based and reanalysis data. Both rings were features with diameters of 200–250 km and geostrophic currents reaching up to 160 cm/s. The ring generated by the first meander facilitated rapid CJT within a few days, while the ring formed at the second meander resulted in a longer transport pathway. The study effectively combines long-term numerical particle tracking and the real-time capture of transient mesoscale features with targeted shipboard observations.

1. Introduction

The Kuroshio Extension (KE) is a zonal eastward flow of the Kuroshio Current formed after this current leaves the coast of Japan at approximately 35–36°N. The KE separates water of subarctic and subtropical structure with different physical and chemical properties. It is a meandering flow (Kawai, 1972) with two quasi-permanent large meanders in the area between the eastern coast of Japan and 155°E (Fig. 1). The western or the 1st meander is located just east of the point where the Kuroshio Current separates from the coast with the northern crest at 144–145°E, and the 2nd meander is situated to the east around 149–150°E (Kawai, 1972; Jayne et al., 2009; Mizuno and White, 1983; Niiler et al., 2003; Yasuda, 2003; Qiu and Chen, 2005; Hirata et al., 2025). These meanders change their position and form in the course of time, but they do not disappear after temporal averaging, presenting, e.g., in climatological maps of the sea surface height (Zhang and Afanasyev, 2023). Both the meanders extend through the entire depth of the ocean and have a significant barotropic component (Yoshikawa et al., 2004; de Verdière & Ollitrault, 2016, Fig. 7).

Strong boundary currents, like the Gulf Stream and the KE, seem to provide an effective barrier to cross-jet transport (CJT). The *permeability of* this barrier and its depth range are debated, and the transport of tracers across it is not fully understood. On the one hand, strong jet currents provide parabolic transport barriers preventing CJT. On the other hand, sparse observations of float tracks (see, e.g., Bower and Rossby, 1989) and simulations using simple models of meandering jet flows (see, e.g., Bower et al., 1985; Budyansky et al., 2009; Uleysky et al., 2010a and b; and a recent review by Prants, 2023) and using satellite-derived surface geostrophic velocity (Liu et al., 2018) show that it is sometimes possible.

URL: http://dynalab.poi.dvo.ru
* Corresponding author.
E-mail address: lebedevamasha671@gmail.com (M.A. Lebedeva).

https://doi.org/10.1016/j.ocemod.2026.102814
Received 2 April 2026; Received in revised form 14 July 2026; Accepted 16 August 2026
Available online 17 August 2026
1463-5003/© 2026 Elsevier Ltd. All rights are reserved, including those for text and data mining, AI training, and similar technologies.

The CJT is important, providing invasion of subtropical and subarctic species into adjacent regions, and for intrusion of water masses with specific properties. Another motivation for studying CJT across the KE appeared after the accident at the FDNPP on March 11, 2011, when a large amount of radioactive water, containing mainly cesium-134 and cesium-137, was discharged into the ocean. Tracking the FDNPP-derived radionuclides' spreading is essential not only for addressing risks of radioactive contamination of the marine environment (Buesseler et al., 2012; Kumamoto et al., 2013; Kaeriyama et al., 2013 and 2014; Budyansky et al., 2015; Kumamoto et al., 2016; Maderich et al., 2024) but also for understanding the transport, mixing, and circulation of water masses in the North Pacific.

The KE weakens as it moves eastward and bifurcates into two or three branches to the east of 155–160°E and then joins subtropical and subarctic gyres. FDNPP-derived radionuclides, advected by the jet to the east, entrain into the western subtropical gyre due to weakness of the transport barrier there. After that, they are advected towards the subtropical area, reaching some Asian marginal seas (Kaeriyama, 2016; Zhao et al., 2021; Kim et al., 2024; Zhang et al., 2025; Liu et al., 2026). In fact, this transport pathway cannot be considered as a CJT. By CJT we mean here the direct transport across the KE where it remains a strong barrier, i.e., to the west of 155°E.

FDNPP-derived radiocesium is a good tracer for detecting CJT. From the end of October to the beginning of November 2012, Kaeriyama et al. (2014) detected relatively high concentrations of Cs^{134} (10–15 Bqm^{-3}) and of Cs^{137}(3–10 Bqm^{-3}) at the depths of 200–400 m in the subtropical region south of the KE at a number of stations along 146 and 147°E transects ranging from 30 to 36°N (see the Table in Kaeriyama, 2016). In the surface layer, concentration of Cs^{137} was in the range of 2–4 Bqm^{-3}. In February 2012, Kumamoto et al. (2014) detected increased concentrations of Cs^{134} (1–7 Bqm^{-3}) andCs^{137}(3–10 Bqm^{-3}) in the surface and subsurface layers at 34.77°N, 148.88°E, south of the KE. They proposed that this signal had originated from isopycnal transport of directly discharged Cs isotopes across the KE. The deepest penetration depth of Cs^{134} (at least 600-m depth) supports the southward transport of Cs^{134}into the subtropical region along isopycnals below the surface mixing layer. The other authors (Yoshida et al., 2015; Aoyama et al., 2016) also observed subsurface maxima of Cs^{134} (>10Bqm^{-3}) in 200–600 m depth starting from about 10 months after the accident. It was concluded that the Fukushima-derived radiocesium was transported not only eastward in surface layer but also southward due to formation and subduction of the mode waters. The preliminary direct altimetry-based simulation (Prants et al., 2014; Cedarholm et al., 2019) also showed that a small number of FDNPP-derived radionuclides could cross the surface KE after the accident. The question is how this could happen, taking into account that the KE is believed to be a transport barrier.

Ikenoue et al. (2023) simulated the dispersion of dissolved radionuclides using long-term reanalysis data and demonstrated that meridional velocity near the FDNPP strongly influences north–south transport, with notable seasonal variations between summer and winter. A recent study by Liu et al. (2026) investigated this discharge starting from August 23, 2023, using a three-dimensional dispersion model. The simulation focused on tritium, covered a dispersion period of over ten years, and was conducted using three years of ECCO2 Cube92 reanalysis data with a horizontal grid resolution of 0.25° and non-uniform vertical discretization (50 layers). By day 3600, most of the surface layer in the North Pacific Ocean had reached tritium concentrations of 0.01 Bqm^{-3} – orders of magnitude below natural background levels (~50 Bqm^{-3}) – with a localized peak near 220°E in the northeast Pacific, suggesting potential radionuclide accumulation in that area. Vertically, tritium concentrations generally decreased with depth. The results indicate that tritium released from the FDNPP primarily disperses eastward along the main path of the KE (35°N latitude). These authors did not, however, focus on the pathways by which the tritium reached latitudes south of the KE, which is the main focus of our research.

We use different diagnostics to detect CJT (Sec. 2). First of all, we calculate the southern and northern components of the altimetric velocity field on a grid for a long period of time with the aim to detect the meridional transport pathways in the KE area (Sec. 3.1). Then, the trajectories of virtual particles, distributed initially at a meridional segment along the coast to the south of the FDNPP site, have been integrated in the altimetric velocity field until they crossed western and eastern zonal segments to the south of the KE. The distributions over the travelling times and dates/coordinates of arrival of the particles, participating in the surface CJT, on the zonal segments have been calculated for a long period of time after the FDNPP accident (Sec. 3.2).

The region of KE is known as an area with high population of anticyclonic and cyclonic mesoscale eddies including the Kuroshio warm-core and cold-core rings pinching off from the KE on both sides (Kawai, 1972; Kitano, 1975; Koshlyakov, 1986; Itoh and Yasuda, 2010; Ueno et al., 2023) (see Fig. 1b and Sec. 3.3.1). Two cyclonic cold-core

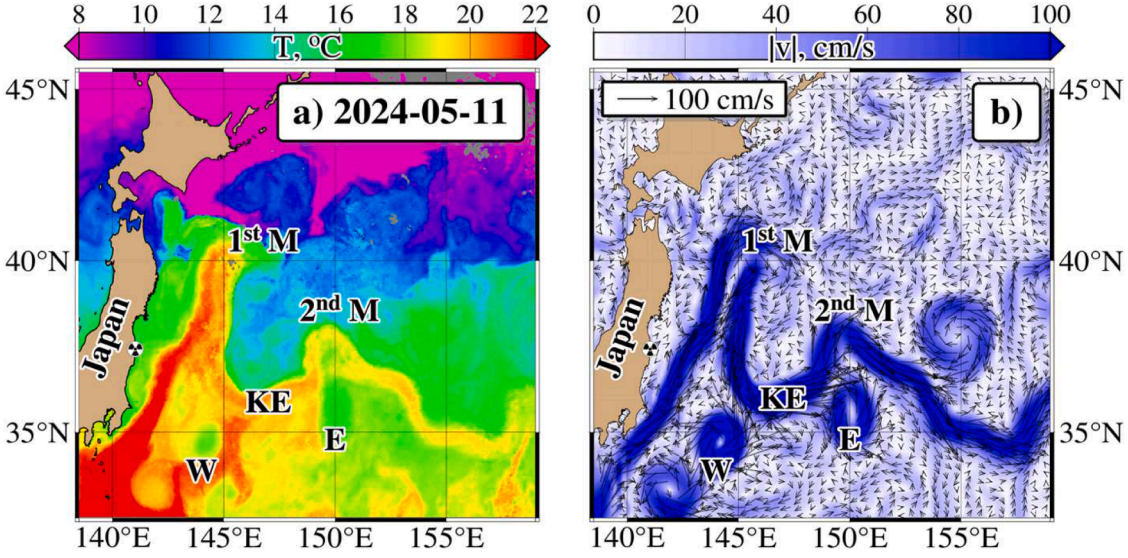


Fig. 1. a) An example of SST distribution on May 11, 2024 in the Kuroshio-Oyashio confluence zone (MODIS on the NASA's Aqua satellite). b) The altimetric velocity field on the same date, showing the path of the Kuroshio Extension (KE) with two meanders (1st M and 2nd M) and cold-core rings E and W. The FDNPP site is marked by the radioactivity sign.

rings have been tracked using the eddy detection algorithm AMEDA in the first half of 2024. They were formed in the beginning of the year at the northern flank, contained a large amount of water from the FDNPP area and then appeared on the southern flank after pinching off from the main jet due to meandering of the KE (Sec. 3.3.2). The tracking of the rings was accompanied by plotting of their thermohaline characteristics using the GLORYS12V1 reanalysis data. The simulated locations of the centers of the rings (elliptic points) have been sent via e-mail to R/V *Akademik Oparin* during the *cruise* No.71 in the study area. This helped to sample the rings on June 22–27, 2024 close to their centers (Sec. 3.3.3) in order to test a ring-assisted mechanism of CJT. The obtained results are discussed in Sec. 4.

2. Data and methods

2.1. Shipboard observations

Ship observations in the study area were implemented during the cruise No.71 of R/V *Akademik Oparin* in June of 2024. The cold-core rings E and W were identified by satellite altimetry and infrared data prior to the cruise (Fig. 1) and then were traced by daily altimetry data. During the cruise, the information on location of KE and the rings was transmitted onboard the vessel in real-time mode (with 1 day delay). The ship made CTD observations along two transects crossing the rings on June 22–24, 2024 (eddy W) and June 25–27, 2024 (eddy E). The ring E located between 33°–34.8°N and 149°–150.5°E was quite stable during the ship observations. A CTD section along 149°45'E from the south to the north crossed it close to the center at 33.9°N. The ring W located in the area of 34°–36°N and 144°–145°E was fast moving in June (see section 3.3). In May it merged with the main stream of KE and became a cyclonic meander. During the ship observations on June 22–23, 2024, it was evolving from elongated cyclonic meander of KE to isolated eddy, thus detaching from KE and shifting to the southwest. Meanwhile, the ship managed to make a meridional CTD transect along 144°40'E from 36°N to 34°N crossing the ring from north to south. Because of fast motion of the ring, part of the transect probably crossed it not exactly through its center but was slightly shifted to the east. The southern part of the transect was turned to the east to escape from strong atmospheric cyclone bringing storm weather.

Along both transects, the distance between CTD stations was around 18–28 km, and the depth of observations was 1000 m. We used SBE-911 CTD system. The data on water temperature and salinity profiles were averaged to 1 m intervals and plotted using the Ocean Data View software (Schlitzer, 2023). Geostrophic velocity was calculated based on CTD data with a reference level of 1000 db.

2.2. Virtual particle tracking

The modeling results in this paper are based on Lagrangian particle tracking (Prants, 2025) in the altimetric velocity field, one of the AVISO/CMEMS products (aviso.altimetry.fr), with the resolution of 0.125° × 0.125° and daily time step. The AVISO product uses corrections for changes in sea level caused by various hydrometeorological phenomena: tides, changes in atmospheric pressure, etc. (for a review see Abdalla et al., 2021). It is convenient to calculate trajectories of tracers by solving advection equations in the following form:

$$\frac{d\lambda}{dt} = u(\lambda, \varphi, t), \quad \frac{d\varphi}{dt} = v(\lambda, \varphi, t), \tag{1}$$

where φ and λ are latitude and longitude of tracers, u and v are the angular zonal and meridional geostrophic velocity components at the marker's location. Bicubic spatial interpolation and interpolation in time by third-order Lagrangian polynomials are used. Trajectories of the tracers are computed by integrating equations (1) using the 4th order Runge-Kutta scheme (for details see Prants et al., 2017). Angular velocities are related to linear velocities by the ratio (Prants et al., 2017)

$$u = \frac{0.864}{1.853}\frac{1}{cos\varphi}U, \quad v = \frac{0.864}{1.853}V, \tag{2}$$

where u and v are expressed in arc minutes per day, and U and V are given in cm/s.

To obtain a statistic of CJT, 5 $\times 10^4$ tracers have been distributed every day from March 11, 2011 to May 16, 2024 over the almost meridional segment in Fig. 1b with the end points 35.6°N, 141°E and 38.2°N, 141.6°E (Sec. 3.2). This segment was located to the south of the FDNPP site, but to the north of the mean position of the KE. To fix the event of CJT, we recorded the number of tracers reaching the western and eastern zonal segments to the south of the KE (see Fig. 1b), the dates and longitudes of arrival of the tracers at these segments. This number of tracers proved sufficient both for identifying transport pathways and for detecting CJT. It is important to note that we do not aim to establish a quantitative relationship between the number of tracers and the actual physical concentrations of radionuclides. The number of tracers is provided solely to identify peaks and arrival times of particles at the specified transects. We reiterate that Lagrangian modeling with trajectory calculations of passive tracers makes it possible to determine the most probable transport pathways of potential contamination and to identify time windows of transport from the shores of Japan to the specified transects.

The data from the GLORYS12V1 eddy-resolving global ocean reanalysis with the spatial resolution of 1/12° and 50 depth levels have been used to calculate thermohaline and other hydrological parameters. These data are available on the CMEMS (Copernicus Marine Environment Monitoring Service) portal, https://data.marine.copernicus.eu/product/GLOBAL_MULTIYEAR_PHY_001_030/description.

It should be noted that the spatial resolution of the altimetric data used (1/8°) and the GLORYS12V1 reanalysis (1/12°) does not allow the reproduction of submesoscale processes (scales less than 10–20 km), which are known to be active in the Kuroshio Extension region and may contribute to turbulent tracer mixing. However, the goal of our work is not to model the full spectrum of turbulence, but to identify the main mechanisms of cross-transport at the meso- and large-scale level. Submesoscale velocity fluctuations can be considered as high-frequency stochastic noise adding extra diffusion to the chaotic advection generated by the mesoscale field. In the absence of large-scale asymmetry in the flow field, such an addition will lead to a more uniform "smearing" of the tracer patch, but will not create a systematic directed flux across the powerful dynamic barrier represented by the Kuroshio jet. Our approach, which uses tracers to reveal coherent transport pathways and time windows, successfully identifies discrete CJT events associated with jet meandering and ring formation, as confirmed by direct shipboard CTD observations (see Section 3.3.3). We therefore consider that the chosen resolution is sufficient for the objectives set in this study.

2.3. The algorithm for detection of eddies and Lagrangian maps

Mesoscale eddies are generated in the Kuroshio-Oyashio confluence zone influencing the pathways of the currents and water transport and mixing in this area (see, e.g., Kitano, 1975; Itoh and Yasuda, 2010 and the recent reviews by Prants, 2021 and Ueno et al., 2023). They are detected here with the help of the Angular Momentum Eddy Detection and tracking Algorithm (AMEDA) based on the altimetric geostrophic velocities (Le Vu et al., 2018) and the GLORYS12V1 reanalysis data. This algorithm determines the polarity, extrema of the local normalized angular momentum, the coordinates of the center, the characteristic radius R_{max}, at which the maximum swirl velocity $V_{max}$is reached, the average velocity on this contour $<V>$, the amplitude and a number of additional characteristics. Only eddies with the lifetime >30 days were considered. We used the recommended settings of AMEDA given by (Le Vu et al., 2018) in their Table 1. The occurrence frequencies of

anticyclonic and cyclonic eddies have been calculated as follows. The study domain was mapped onto a 0.1° × 0.1° grid, and the vortex contours were identified daily in the velocity field. The number of occurrences, in which each grid point was included within a vortex contour, was then calculated and normalized to the total number of days during the observation period, from January 1, 1993 to December 31, 2024.

The length of trajectory of each marker on the Earth's sphere is calculated by integrating advection equations (1) backward in time as follows (Ponomarev et al., 2018):

$$L = R\int_0^T \sqrt{(\lambda'(t))^2\cos^2\varphi(t) + (\varphi'(t))^2}\, dt. \quad (3)$$

Here $\varphi'(t)$ and $\lambda'(t)$ are time derivatives, R=6371 km is the Earth's radius. The values of L in km are represented on Lagrangian (L-) maps by gradation of grey color. These maps are parameterized by the starting date and the integration time T. The L-maps show the value of L for each marker for T=30 days prior to the date indicated on the map. The consecutive maps allow us to track evolution of eddies and to document the processes of entrainment and detrainment of water by eddies.

3. Results and discussion

3.1. The transport pathways in the Kuroshio Extension area

The spatial distributions of the southward (negative) and northward (positive) components of the interpolated altimetry-derived velocity vs longitude demonstrate two peaks (Fig. 2). The data were calculated along the 35°N latitude on a 0.1° × 0.1° grid and averaged for 32 years. Fig. 3a and b give a pattern of the distribution of the velocity components vs longitude. This simple metrics highlights the quasi-permanent meridional transport pathways in the KE area by increased values of the southward component of the surface velocity in the ranges of 144–146°E and 150–152°E, whereas the increased values of the northward component occur approximately in the ranges of 141–143°E and 146–150°E. This proves a pretty stable position of the 1st and 2nd meanders of KE in spite of the reported interannual variations (Mizuno and White, 1983; Qiu, 2002; Qiu and Chen, 2005).

3.2. Direct modeling of cross-jet transport

3.2.1. The western passage

To study the possibility of CJT, a total number of 5 ×10^4 tracers has been launched in the FDNPP area every day from March 11, 2011 to May 16, 2024 along the magenta segment in Fig. 4 located just to the north of the mean position of the KE. The longitudes and dates of arrival of these tracers at the western zonal segment (WS) (Fig. 4) to the south of KE mean position have been recorded. Each such event is considered as a CJT. The majority of tracers reached the segment in the range of 144–146°E (Fig. 5a) in accordance with the mean position of the 1st meander and with the increased values of the southward component of the altimetry-derived speed of currents in this range (Fig. 3a). Distribution of the tracers, reaching the western segment, over the travelling time is shown in Fig. 5b. The majority of tracers reached the segment within a month after launching.

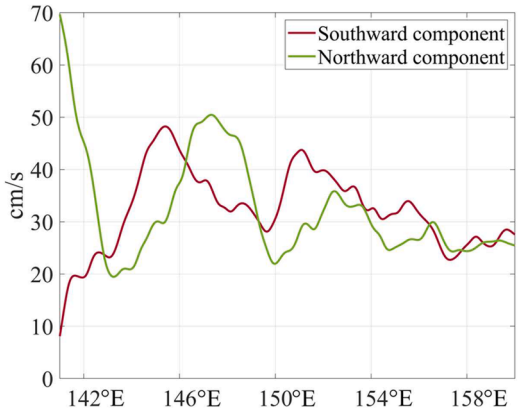


Fig. 2. The values of the southward (brown) and northward (green) components of the altimetry-derived speed of currents vs longitude. The data were collected along the 35°N latitude and averaged from January 1, 1993 to December 31, 2024.

Fig. 6a shows the longitude of tracers' arrival to the western segment depending on their arrival date during 2011–2024. It shows that the corridors for CJT 'open' during short periods of time, when the tracers reach the western segment simultaneously. The direct evidence of that is illustrated by Fig. 6b where the tracers are distributed over the dates of arrival at the segment. Fig. 6c shows the distribution of the dates of launching. The distributions over the dates of arrival and the dates of launching well correlate with each other (see also Fig. 1S in Supplementary material) with a shift in dates due to the time the tracers need to reach the segment from different places. That means that CJT is the event when large portions of tracers coherently cross the jet during a short interval of time when the corridors of possibility open.

The chosen algorithm for identifying CJT episodes has a drawback, because the obtained statistics on the tracers reaching the designated segments contain information about the fluctuations of the KE jet, during which the tracers cross the segment without CJT occurring. However, even in such a situation, the obtained information on the times and coordinates of the tracers reaching the segments is sufficient to identify the time periods when CJT occurs (see Fig. 6), which is a convenient and fast way to search for CJT episodes over a long period of time. Formally, real CJT can be separated from jet fluctuations by discarding episodes where the coordinates of tracers reaching the western segment form groups with longitudes from 142°E eastward in Fig. 6a.

Our study is exclusively focused on the horizontal transfer of tracers. As shown in Figs. 5 and 7, the advection of the vast majority of particles from the FDNPP area to the segments ranges from 20 to 100 days. In dynamically active regions (at mesoscale fronts), vertical velocities are in the range of 0.1 - 1 m/day, and the vertical displacement of a particle over 100 days is in the range of 10–100 meters. Thus, the particles remain in the surface layer throughout this period, and their vertical position does not affect their horizontal trajectory within the framework of the problem under consideration.

3.2.2. The eastern passage

The similar calculations, as in the preceding section, have been carried out for the tracers reaching the eastern zonal segment (ES) located two degrees southward from the western one (Fig. 4). The majority of tracers reached the segment in the range of 148.5°–149°E (Fig. 7a) in accordance with the mean position of the 2nd meander and with the increased values of the southward component of altimetry-derived speed of currents in this range. The plot of their travelling time has two peaks, one around 30–40 days after launching, and another one around 80–90 days after launching.

The plots in Fig. 8 show that tracers, as a rule, arrive at the eastern segment on certain dates as groups consisting of 2,000–5,000 particles. We could count around 10 events of CJT during a long period of time, from March 11, 2011 to May 16, 2024. Similarly to the western segment, the distributions over the dates of arrival and the dates of launching have a good correlation with each other (Fig. 2S in Supplementary material).

The number of tracers that crossed the western segment is much higher than the number of those that crossed the eastern segment (Figs. 5 and 7). The reason is that the western segment is located closer to the FDNPP site, so the tracers reach the first meander of the KE faster and are then transported southward to the western segment. Fig. 5

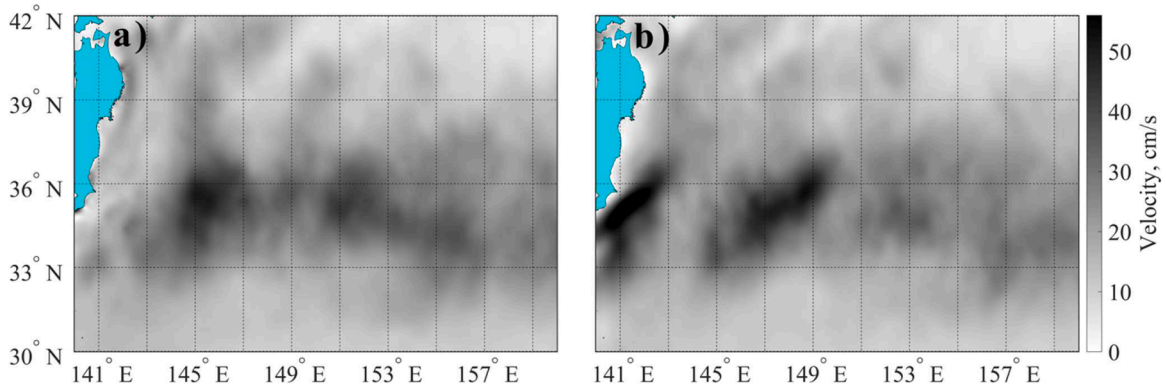


Fig. 3. The spatial distribution of a) the southward (negative) and b) the northward (positive) components of the geostrophic velocity in the Kuroshio Extension area averaged from Jan. 1, 1993 to December 31, 2024.

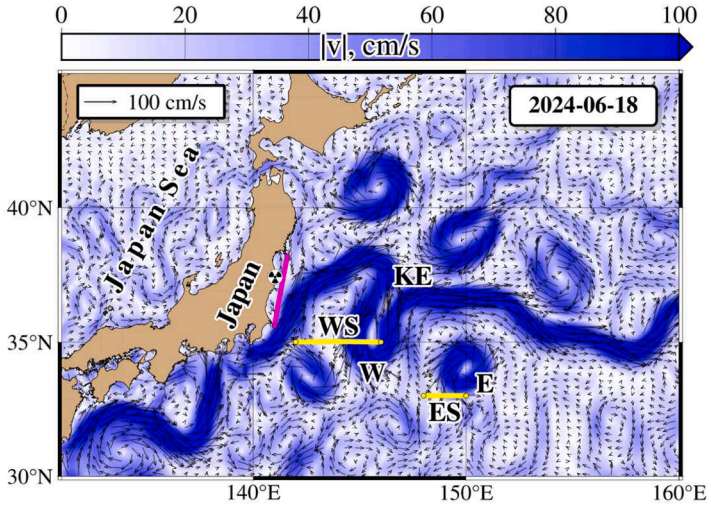


Fig. 4. The altimetry-based velocity field in the Kuroshio Extension area with cold-core and warm-core rings on June 18, 2024, just before ship observations on June 22–27, 2024. Tracers were launched along the magenta segment and detected on the western and eastern zonal segments (yellow sections). The FDNPP site is marked by the radioactivity sign. KE – main jet of Kuroshio Extension. E and W – cold core rings, WS – western zonal segment, and ES – eastern zonal segment.

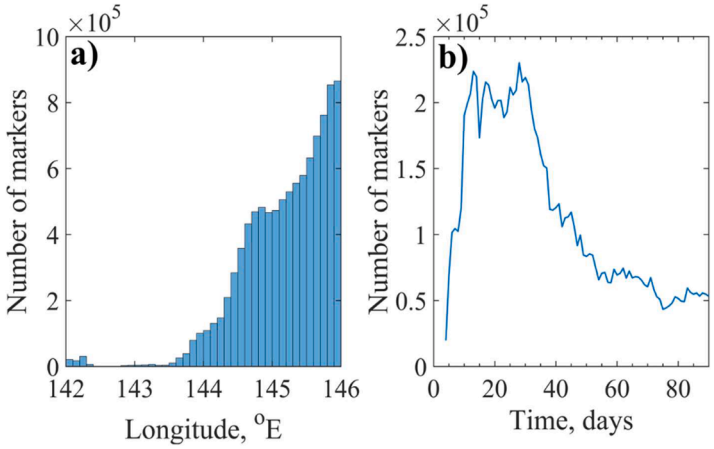


Fig. 5. a) Distribution of tracers launched at the magenta segment in Fig. 4 from March 11, 2011 to May 16, 2024 over the longitudes of their arrival at the western segment (WS) in Fig. 4 and b) distribution of tracers reaching this segment over their travelling time.

shows that the majority of tracers reach this segment within 30 days. The remaining tracers are transported eastward along the KE and may become trapped by the second meander after 40–90 days.

3.2.3. CJT by meandering of the Kuroshio Extension and ring formation

Figs. 6 and 8 show that the process of CJT has no clear periodicity associated with seasonal variations and depends on irregular phenomena such as the intensity of KE meandering. One may expect that the

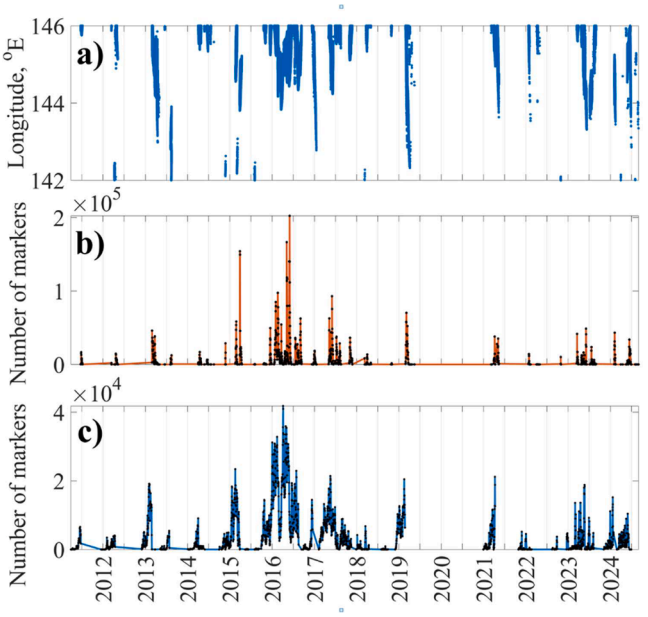


Fig. 6. a) Longitudes of tracers' arrival at the western segment over the dates of their arrival during a long period of time and b) distributions of number of these tracers over the dates of arrival and c) launching.

stronger the meandering of the KE jet, the more tracers will cross the jet southward. The northern edge of the KE may be identified as a strong temperature front clearly seen at the temperature maps at 200 m depth presented in Fig. 9. This figure demonstrates a few examples of different patterns of KE meandering. As it was shown above (Figs. 6c and 8c), at the beginning of 2013, a large number of tracers launched in the FDNPP area crossed both the western and eastern segments. This period corresponds to a period of intense meandering of the KE and the formation of strong cyclonic rings (Fig. 9a). The large 1st cyclonic meander of the KE around 143–145°E was extended far southward down to 32–33°N, thus allowing FDNPP tracers to be transported from the northern side of the KE jet to the south across the western segment, located along 35°N. The following formation of a strong cold-core ring and its detachment from the KE jet continued to transport tracers southward across the segment. During the same period, strong cold-core rings formed in the area of the 2nd meander and then travelled westward, crossing the eastern segment located along 33°N.

In contrast, during the year 2020, we did not observe any notable CJT of tracers (Figs. 6 and 8) and KE meandering was very weak (Fig. 9b). The KE front was located to the north of 35°N, to the north of the western segment (Fig. 9b). Three cold-core rings were observed in the area between 33–35°N and 140–150°E. Westward propagation of the rings formed in the eastern area may have caused the CJT event observed at the eastern segment at the beginning of 2020. However, these rings did not cross the western segment located to the north of their trajectories. Consequently, no signal of CJT was recorded at the western segment during this period.

Another pattern of KE meandering was observed in the spring of 2024 (Fig. 9c). The 1st anticyclonic meander of the KE (142–145°E) was well developed and propagated far to the north. In April 11–20, 2024, the figure shows a detachment of a warm-core ring from this meander. However, a few days later the ring was absorbed by the KE intrusion and finally detached in the middle of May (not shown). To the south of the KE, two strong cold-core rings were observed. Ring W, located around (34°N, 144°E), was formed from a cyclonic meander developed in early 2024 and then it contacted KE a few times and detached again. This provided a peak in tracer transport across the western segment in 2024 (Fig. 6c). Similarly, another cold-core ring, ring E, located around (35°N,

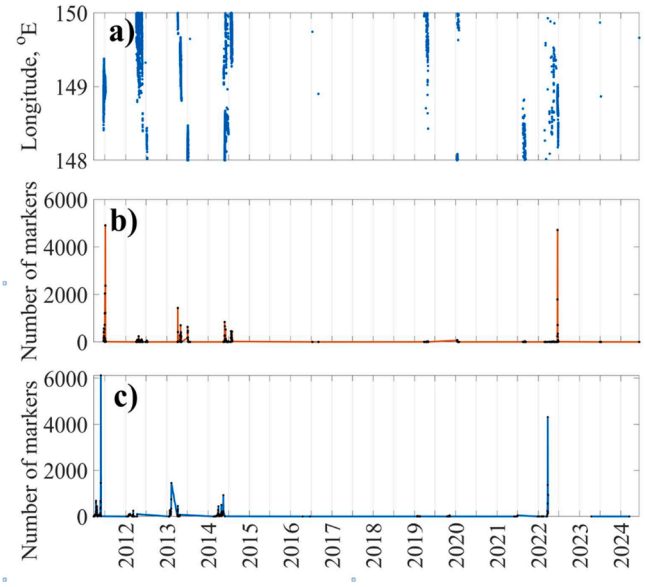


Fig. 8. a) Longitudes of tracers' arrival at the eastern segment over the dates of their arrival during a long period of time and b) distributions of number of these tracers over the dates of arrival and c) launching.

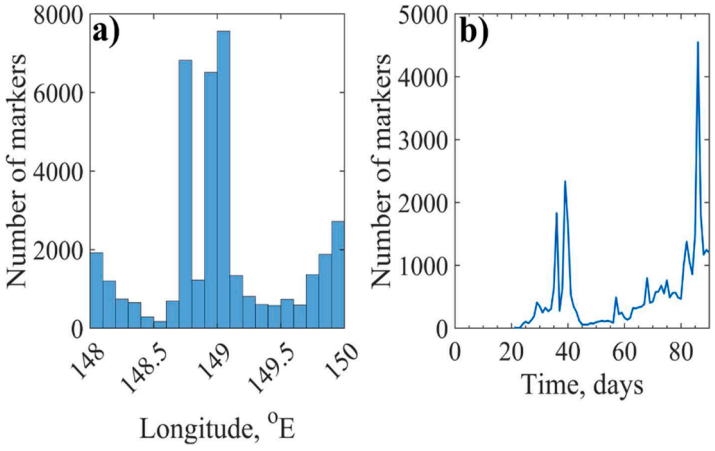


Fig. 7. a) The distribution of tracers, launched at the magenta segment in Fig. 4 from March 11, 2011 to May 16, 2024, over the longitudes of their arrival at the eastern segment (ES) in Fig. 4 and b) distribution of tracers over their travelling time.

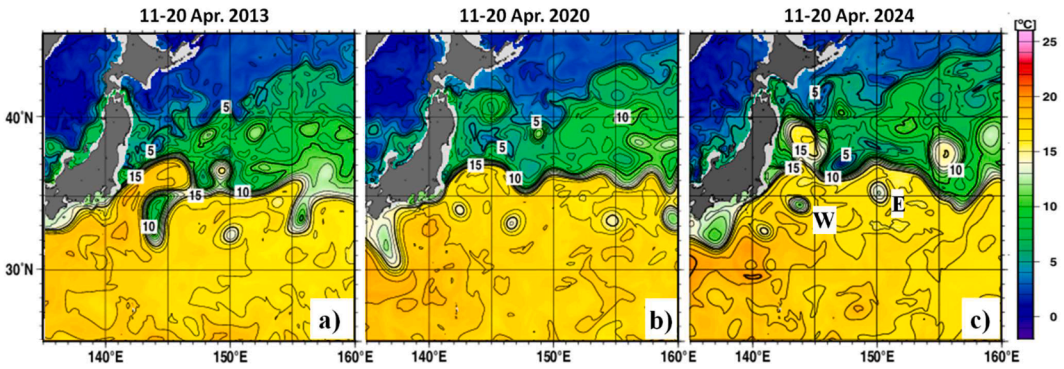


Fig. 9. 10-days mean distribution of water temperature at 200 m depth based on Japan Meteorological Agency data (www.data.jma.go.jp) for April 11–20 of a) 2013, b) 2020 and c) 2024 demonstrate different patterns of Kuroshio Extension meandering: a) large cyclonic meanders and cold-core rings formation, b) weak meandering and c) large first anticyclonic meander and strong cold-core rings E and W south of KE jet.

150°E) in April 2024, moved southward, crossing the eastern segment and thus providing CJT there (Fig. 8c). The structure and evolution of these two rings are discussed in the following sections.

Long-time observation of tracer trajectories allows us to conclude that two mechanisms of CJT can be identified. The majority of tracers that reached the western segment did so within a month after launching. This short travelling time can be partly explained by the following observations. Some tracers reach the northern KE flank, and may eventually cross the western zonal segment due to the developing of the 1st KE meander. After detachment of a cold-core ring from this meander, part of these tracers remains in the subtropical area. However, some KE meanders do not split off from the KE; they do not produce rings but they return northward to their previous position. In this case, no real CJT occurs even if it was formally registered by our calculations above and the tracers reached the segment. The tracers arrive at the segment and cross it when a meander grows southward. However, they then move northward with the retreating meander and remain on the northern flank of the KE. A real CJT occurs when a cold-core ring detaches from the growing meander because the ring traps the water with FDNPP markers from the north of the KE and transports it to the southern area. The ring-assisted mechanism of CJT will be considered in Sec. 3.3. In both cases, the Fukushima-derived radionuclides or other tracers may end up on the other side of the KE.

The short-period dynamics play a dominant role in tracer transport to the segments. Nevertheless, Figs. 2 and 3 provide useful information, as they illustrate the quasi-stationary structure of large-scale flows, which sets the corridors for subsequent transport. As shown in these figures, the current field, averaged over a 32-year period (1993–2024), clearly demonstrate the presence of two stable KE meanders and the associated meridional transport corridors, through which particle transport from the FDNPP to the KE predominantly occurs. This simple metric highlights quasi-permanent meridional transport pathways in the KE region: (i) enhanced southward components of surface velocity are observed in the range 144–146°E and 150–152°E; (ii) enhanced northward components are observed in the range 141–143°E and 146–150°E. Thus, despite well-known interannual variations (Mizuno and White, 1983; Qiu, 2002; Qiu and Chen, 2005), the positions of the first and second KE meanders remain fairly stable on average. It is these stable transport corridors, identified in Figs. 2 and 3, that determine the longitudinal localization of transport, against which short-period variability subsequently develops.

3.3. The ring-assistant mechanism of cross-jet transport

In this section, we combine long-term numerical particle tracking and the real-time capture of transient mesoscale features with targeted shipboard observations.

3.3.1. Mesoscale eddies in the Kuroshio-Oyashio confluence zone in the altimetry era

The Kuroshio-Oyashio frontal zone is the region populated with anticyclonic and cyclonic eddies (see, e.g., Kawai, 1972; Kitano, 1975; Koshlyakov, 1986; Itoh and Yasuda, 2010; Prants, 2021; Ueno et al., 2023). The rings, mesoscale eddies pinched off from the KE, are distinguished by their size and lifetime. Fig. 10 highlights the eddy activity in the region by calculating the occurrence frequencies of mesoscale anticyclonic and cyclonic eddies with the help of AMEDA in 1993–2024, as it is described in Sec. 2.3. The eddies more often occur at the locations of the 1st and 2nd meanders, in the ranges of 142°–144°E and 147°–149°E. The increased densities of tracks of anticyclones (Fig. 3Sa) and cyclones (Fig. 3Sb) are observed along the primary meridional pathways in Fig. 3. The eddies in the Kuroshio-Oyashio frontal zone are coherent features with the median lifetime equal to 51 days for anticyclones and 48 days for cyclones (Fig. 11).

3.3.2. The role of rings in cross-jet transport

Kuroshio rings with diameters in the range of 100–300 km play a crucial role in water mass transport, heat and salt fluxes, transport of nutrients and influence primary production, nitrogen cycling, and carbon fluxes in the North Pacific (for a recent review see, e.g., Ueno et al., 2023). The warm-core rings, which are mostly anticyclonic, detach from the northern flank of the KE, while cold-core eddies, which are mostly cyclonic, detach from its southern flank (see, e.g., Kawai, 1972; Kitano, 1975; Itoh and Yasuda, 2010; Prants, 2021; Ueno et al., 2023). Under the influence of the beta effect, they migrate westward. Most KE rings are eventually reabsorbed by the main jet.

The high values of the nonlinear parameter $\eta = V/c$ (Flierl, 1981) with the median values equal to 2.7 for anticyclones and 2.9 for cyclones imply that tracers trapped in the vortex cores are advected with the eddy for a long time as it translates (see direct evidence of that in Udalov et al., 2024). Here V is the maximum swirl speed, and c is the mean translation speed of the eddy. In what follows, we will use virtual particles released after recent discharges from the FDNPP site as tracers, allowing us to document the events of CJT for a long time. A significant number of FDNPP tracers has been launched daily during the eight episodes of discharging purified radioactive water into the ocean.

Here, we will consider tracers' transport by two cyclonic cold-core rings, W (western) and E (eastern), located to the south of the KE (Fig. 12). The main stages of evolution of these rings are illustrated with the help of Lagrangian L-maps in Fig. 12. The ring W started to form in the beginning of 2024 on the northern KE flank after the appearance of an elliptic point inside the loop-like 1st meander and a hyperbolic point at the base of the loop (Fig. 12a). The ring pinched off from the main jet on the southern flank at the end of February (Fig. 12b). During March and April, the ring was an isolated feature, surrounded by subtropical waters to the south of the KE (Fig. 12c). However, it was absorbed by the

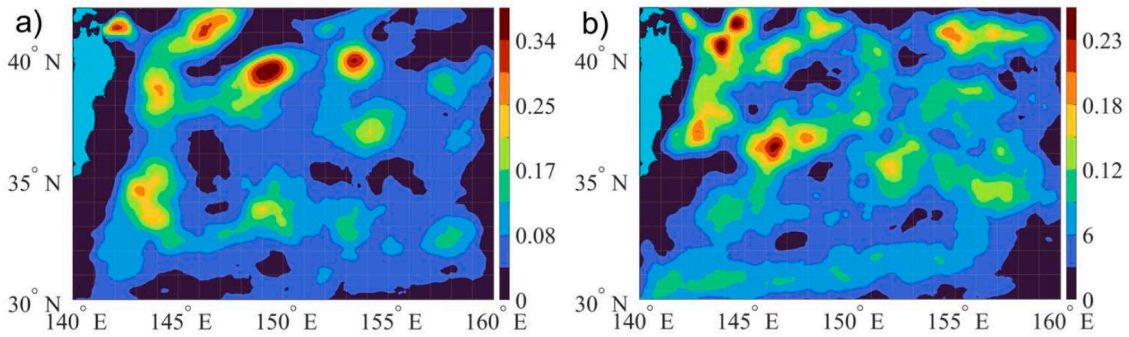


Fig. 10. The occurrence frequencies of mesoscale a) anticyclonic and b) cyclonic eddies in the Kuroshio-Oyashio confluence zone with the lifetime >30 days calculated using the AMEDA from January 1, 1993 to December 31, 2024.

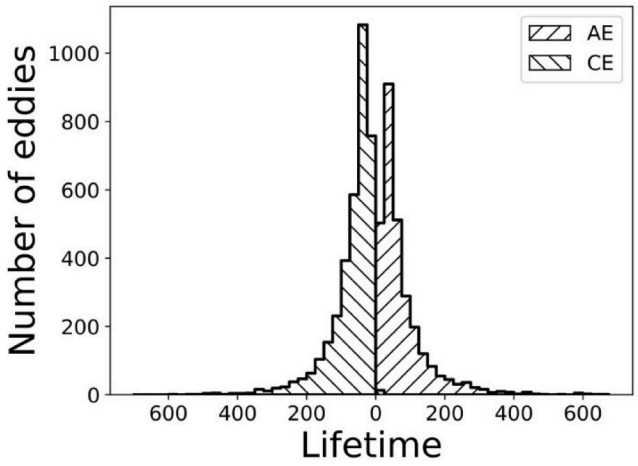


Fig. 11. Distribution of anticyclones and cyclones in the Kuroshio-Oyashio confluence zone over the lifetime (1993–2024).

KE jet in May for a while (Fig. 12d). The splitting process started again in June, and the ring W eventually pinched off just before sampling (Fig. 12e and f).

The ring E started to form simultaneously with the ring W but inside the 2nd meander around 151°–153°E (Fig. 12a). It was formed completely by the end of February (Fig. 12b) and then pinched off from the KE jet, drifting westward (Figs. 12c, d, e and f). The L-maps in Fig. 12 show the spatial distribution of the tracers launched along the magenta segment starting from the first purified water discharge at FDNPP on August 24, 2023. The majority of tracers have been transported eastward, but some of them were detected inside the rings W and E, which eventually pinched off from the 1st and 2nd meanders, respectively, and drifted westward. These rings trapped the tracers and played the role of 'carriers', transporting tracers from the FDNPP site to the south across the KE jet. It should be noted that before May there were not many tracers observed in the core of ring W (Fig. 12b and c). However, after the ring re-contacted the KE in May and detached from the KE in June, the number of tracers increased significantly (Fig. 12d, e and f). This suggests that the large number of tracers was trapped by the ring after its repeated contact with the KE.

The KE jet represents a powerful dynamic barrier to meridional transport. Its high velocity gradients effectively restrict exchange between the northern and southern sides. Therefore, the presence of tracers south of the KE should *a priori* be negligible. This is not an anomaly, but a regular feature. The particles that do manage to cross the jet do not diffuse uniformly through it. Instead, they are transported discretely, namely, within the cores of cyclonic rings that detach from the KE. It is precisely the rings W and E that capture the tracers and carry them southward. This process is clearly illustrated in Fig. 12a–d. The absence of a continuous tracer field south of the jet accurately reflects the role of the KE as a barrier with episodic "transport windows" in the form of eddies.

3.3.3. Sampling of the cyclonic ring W and E

Two CTD transects across the rings W and E were implemented by R/V *Akademik Oparin* during June 22–27, 2024. Their locations are shown in Fig. 12. A few days before sampling, ring W was still merged with the KE, and its cold core area was connected with cold waters of the confluence zone north of the KE front as an elongated meander. Then, just a day before sampling, it detached from the KE jet and moved rapidly to the southwest. As a result, the CTD section along 145.67°E may have crossed the ring not exactly though its center but was slightly shifted to its eastern side.

The CTD measurements along this transect in June 22–24, 2024 (Fig. 13) show that the core of the ring contains denser, colder and fresher water compared with the surrounding. The ring W represented quite a strong dynamic feature. The central part of the ring had a dome-like structure with isolines shifted up by 500 m in comparison with the surrounding waters. The temperature difference between the ring center and surrounding water in the layer 100–500 m was around 9–10°C. In its core, the ring contained an extremely low salinity water (33.7–33.9) at intermediate depth (200–500 m), trapped from the confluence zone area north of the KE (Fig. 13b). This low salinity water provided a negative density anomaly in the ring center (Fig. 13c) and resulted in cyclonic geostrophic rotation of the ring. Very strong geostrophic currents exceeding 160 cm/s were observed at the eastern edge of the ring (Fig. 13d). Strong currents up to 20 cm/s were traced down to a depth of 650 m.

In the surface layer (0–100 m), the ring contained colder and lower salinity water in its center (18–19°C and 34.2–34.3) and a warmer belt (22–23°C and 34.5–34.6) surrounding the core, a remnant of the KE water which forms a ring-like structure of such eddies. The cold and low salinity water inside the ring has properties similar to those of the water just to the north of the KE in the confluence zone. This proves intrusion of confluence zone water into the ring when it was connected with the KE during May-June and the advection of more tracers during this period. Then, after the ring detachment, the tracers were trapped in its core and were transported across the KE front with the ring.

Another CTD transect along 149°45'E, implemented in June 25–27, 2024, crossed the eastern cold-core ring E and the main jet of the KE from south to north (Fig. 12). Similar to the western ring W, the CTD measurements show that the core of the ring E contained colder, less saline and higher density water compared with the surroundings (Fig. 14). However, the temperature and salinity contrasts of this ring were slightly lower than those of the western one. The elevation of isolines in the center of ring E may be estimated as 300–400 m compared with more than 500 m in ring W. The temperature difference between the ring center and the surrounding water in the 100–500 m layer was around 5–6°C. The ring contained low salinity water in its core

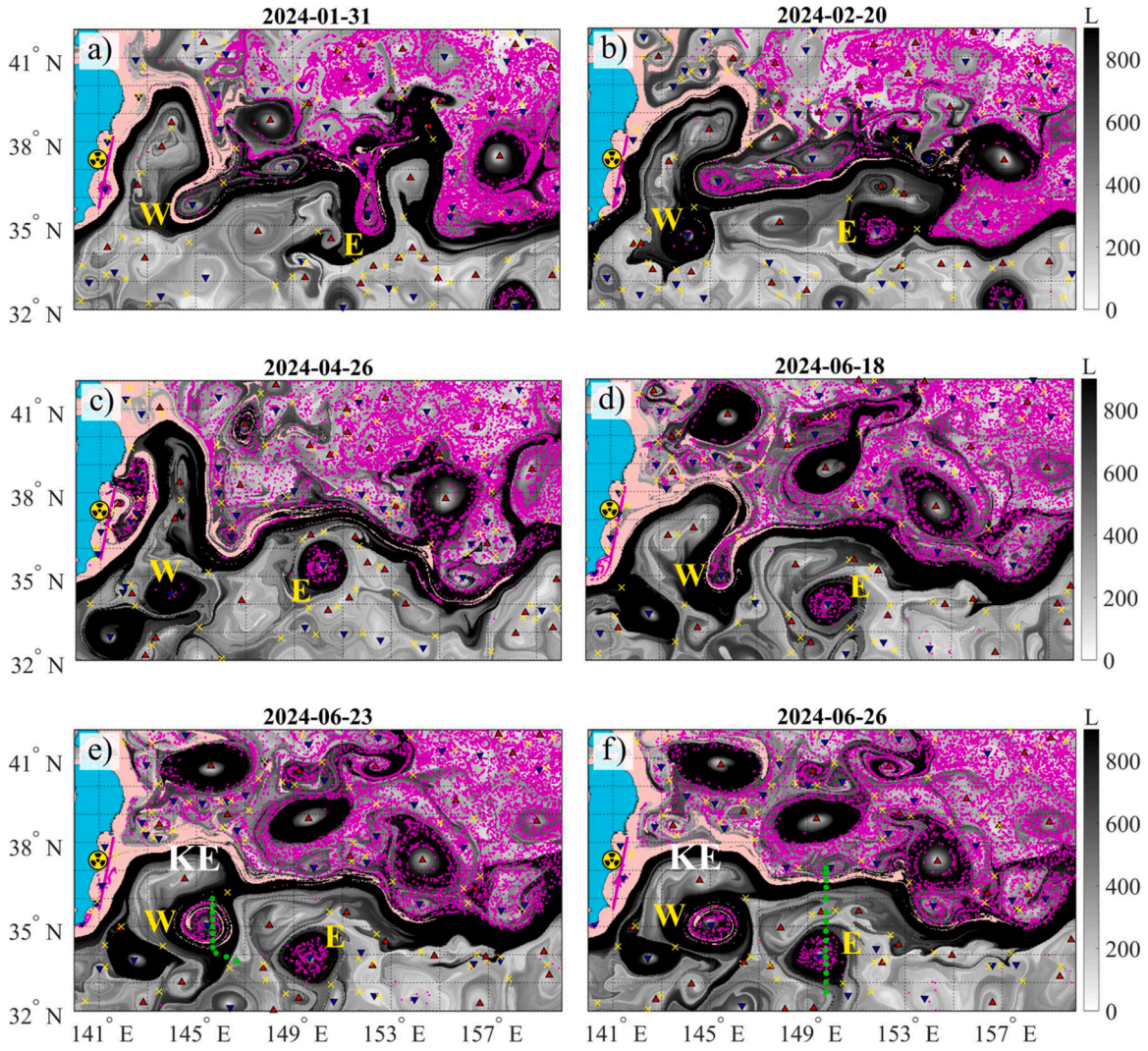


Fig. 12. The consecutive Lagrangian maps with the tracer distribution illustrate the process of formation and evolution of the cold-core rings W and E from January 31 till June 26, 2024. Both rings started to form simultaneously inside the 1st and 2nd meanders. a) the formation stage; b) the first pinch-off from the main jet on the southern flank; c) isolated period of both rings; d) absorption of the ring W by the KE jet, while ring E remained isolated from the KE and drifted westward. e, f) the ring W eventually pinched off from the KE jet just before sampling. The path *L* in km covered by the tracers prior to the indicated dates is color-coded in shades of gray. Light pink color indicates coastal water. Green dots are the locations of CTD stations by R/V *Akademik Oparin* in June 22–27, 2024.

(400–600 m); however, salinity values were not as extreme and varied between 33.8 and 34.0 (Fig. 14). As a result, the geostrophic currents were quite strong and exceeded 100 cm/s at the southern edge of the ring and 80 cm/s at its northern edge, but they were slightly lower than those in ring W.

The transect also crossed the main KE jet (Fig. 14). It was clearly visible in the geostrophic velocity field as a narrow zone (around 100 km) of strong currents exceeding 120 cm/s. The same width of the KE jet may be estimated from the Lagrangian maps (Fig. 12). The KE jet has a very sharp front on its northern side with temperature and salinity difference around 10°C and 0.7 psu, respectively, at a depth of 100 m. The southern side of the KE had no sharp contrast and was visible only in the upper 0–75 m layer as a warmer (>24°C) and less saline (34.2–34.3) water area. Lower salinity water similar to the KE's northern edge was observed at the surface layer of the ring E, which indicates a possibility of trapping the tracers from the confluence zone by this ring.

Both rings W and E are strong dynamic features. Their diameters may be estimated as 200–250 km based on CTD transects (Figs. 13 and 14) and Lagrangian maps (Fig. 12). T-S anomalies associated with rings were traced down to the maximum depth of observations, which suggests that the rings penetrated deeper than 1000 m. Strong currents up to 20 cm/s were observed down to 600–650 m depth. Very strong currents (120–160 cm/s) in the surface layer are comparable to and even exceeding the flow of KE jet (Figs. 13 and 14). Western ring W shows a stronger anomaly in T-S characteristics and currents than eastern ring E. This is probably caused by its recent contact with the KE and intrusion of water from the confluence zone north of the KE. This could result in advection of newer FDNPP tracers into the ring. Eastern ring E was isolated from the KE for a few months. Thus, its core water has been slightly modified during the ring's evolution.

The observed cold-core rings are similar to strong rings of Kuroshio observed in this area in previous studies (Masuzawa, 1957; Cheney et al., 1980; Kawai, 1980; Tomosada, 1984; Koshlyakov, 1986; Xi et al., 2018; Nakajima et al., 2024). Thus, we may expect that CJT events caused by cold-core rings are typical phenomena for this area. Strong rings produced by the 1st meander provide fast CJT and transport of FDNPP tracers across the KE within a few days, as was observed by our tracer experiment. Longer transport could be provided by rings formed at 2nd meander. By contacting the KE a few times, merging and detaching again, the rings provide multiple events of CJT.

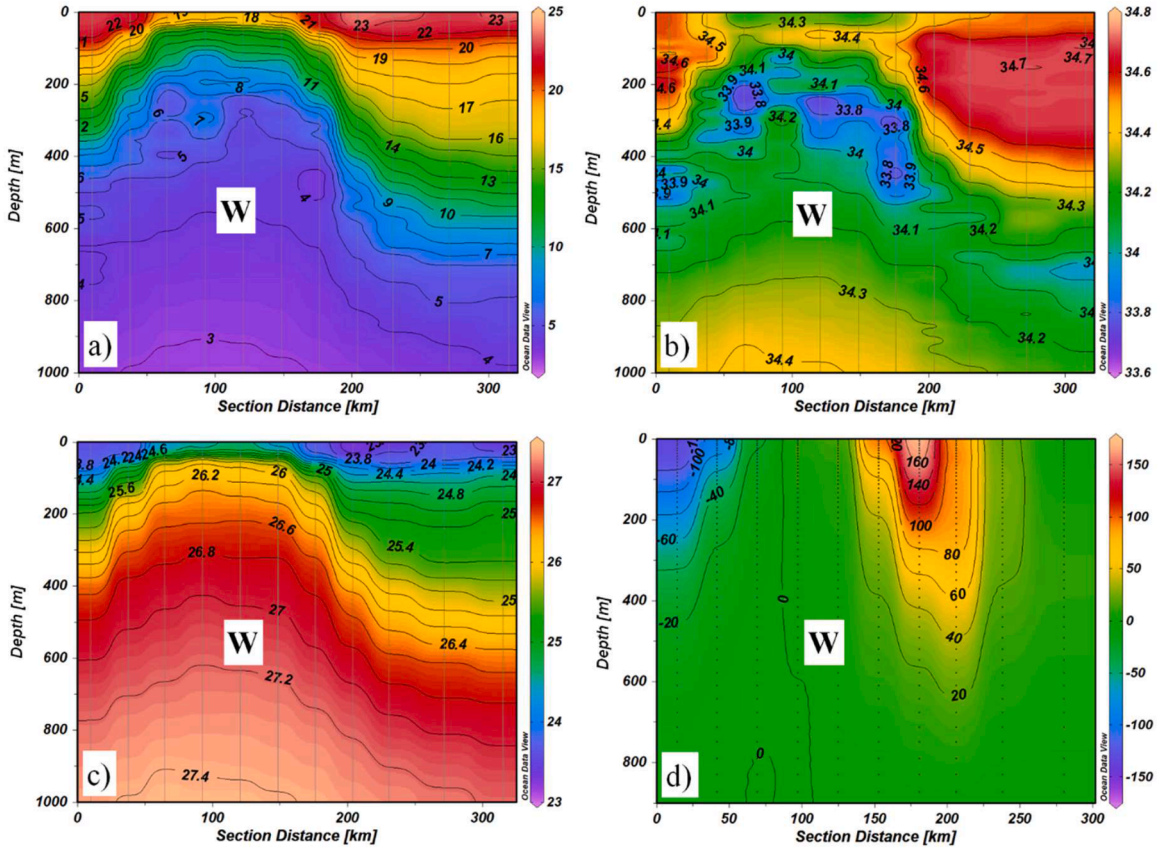


Fig. 13. Vertical distribution of a) water temperature (°C), b) salinity, c) density anomaly (kg/m3) and d) geostrophic velocity normal to the section (cm/s) along the CTD transect crossing cold-core ring W on June 22–24, 2024. Vertical lines represent CTD casts. North is on the left. Locations of the stations are shown in Fig. 12e.

3.3.4. Changes in the thermohaline structure of the cyclonic ring W during its evolution

In this section we have examined changes in the thermohaline vertical structure of the sampled rings using the GLORYS12V1 reanalysis data. The surface velocity field is shown in Fig. 15a just after formation of ring W inside the 1st meander. The beginning of the formation process is signaled by the appearance of an elliptic point in the vortex center and a hyperbolic point on its periphery (Fig. 15a). The GLORYS12V1 data on February 9, 2024 show a typical vertical structure for cyclonic eddies with *dome-like* isolines in their centers and higher density, colder, and fresher core water of subarctic origin compared with the surrounding waters (Fig. 15b, c and d). Just after detaching from the KE, the ring demonstrated a strong anomaly in T and S fields. A 10°C isotherm was shifted up to 50 m in the ring center (Fig. 15b). A layer of intermediate low salinity water (33.7–34.25) was located very close to the surface, between 50 and 200 m (Fig. 15c). The isopycnal line 26.0 was shifted from 500 m in the surrounding waters to 50 m in the ring center (Fig. 15d).

Middle and lower panels of Fig. 15 illustrate the changes in the vertical structure of ring W during 4.5 months of its evolution from the formation to ship sampling on June 23. After separation from the KE in February, the ring was evolving as an isolated structure. By the end of April, it slightly lost its anomaly (Fig. 15e, f, g and h). Its core water became warmer and more saline. The most notable changes happened in the upper 300–400 m layer. A 10°C isotherm shifted down to 300 m and minimum salinity became higher than 34.2. However, it kept a strong dynamic anomaly by high elevation of isopycnals at its center (Fig. 15h), similar to what was observed in February.

In May, cold-core ring W merged with the KE again and separated in June 18–23, just before the ship survey. The lower panel of Fig. 15 shows the ring structure just after its second separation from the KE. The ring received a portion of fresh, cold, and low salinity water from north of the KE. The 10°C isotherm jumped up to 150 m, and salinity decreased below 34.0 at its center. The isopycnal line 26.0 was located around the same high position (100 m) in the ring center, confirming cold-core ring W to be a strong dynamic feature.

Fig. 16 shows the evolution of the thermohaline structure of cold-core ring E, also based on GLORYS12V1 data. T-S anomaly in the subtropical waters associated with ring E was quite significant but slightly smaller compared with ring W. In February, just after its formation, a 10°C isotherm in its center was located around 280 m, a low salinity layer (33.9–34.1) occupied 250–600 m, and the 26.0 isopycnal line was around 180 m (Fig. 16b, c and d). After separation from the KE, the ring slowly decreased; however, its parameters by the end of April (Fig. 16f, g and h) were not much lower compared with February. A more notable decrease was observed by the end of June (Fig. 16l, m and n).

Comparison of GLORYS12V1 data (Fig. 15l, m and n and 16l, m and n) with ship CTD observations shows very good agreement for the structure of both rings. Presenting a realistic general structure of the rings, the GLORYS12V1 data provide a smoother picture of the rings' T-S extremes, smoothing them by 50–100 m. However, it presents quite realistic evolution of the rings' structure. The data show slow dissipation of T-S anomaly associated with the ring after its separation from the KE and an increase in the ring's strength after a second contact with the KE, which provides a new fresh water intrusion into the ring center.

4. Conclusions

The main results of this study are the following. The dominant meridional transport pathways in the KE area have been found, quantified by increased values of the southward and northward components of the geostrophic velocity in the last 32 years. They are connected with

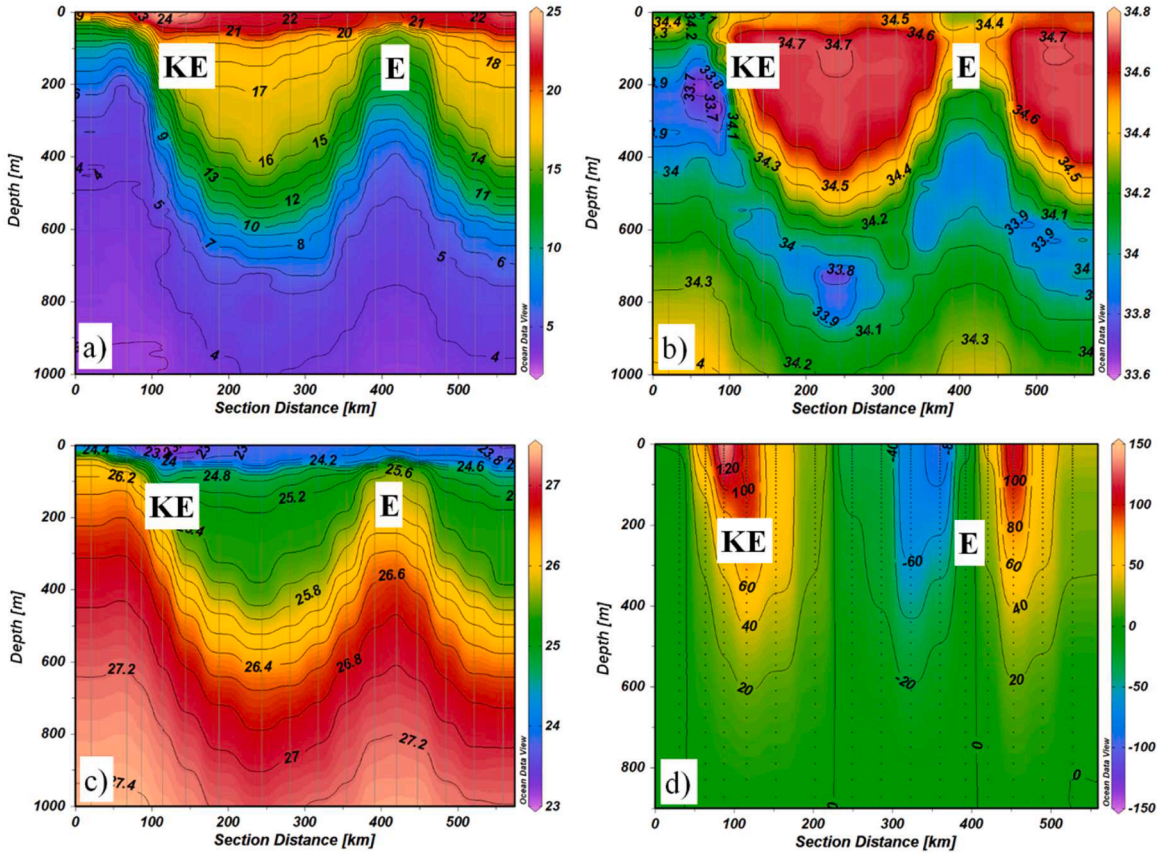


Fig. 14. Vertical distribution of a) water temperature (°C), b) salinity, c) density anomaly (kg/m^3) and d) geostrophic velocity normal to the section (cm/s) along the CTD transect crossing cold-core ring E on June 25–27, 2024. KE – main jet of Kuroshio Extension. Vertical lines represent CTD casts. North is on the left. Locations of the stations are shown in Fig. 12f.

the mean locations of two KE meanders. Virtual tracers launched in the area around the FDNPP site can cross the KE jet moving southward along these transport corridors. Two mechanisms of CJT have been identified. The FDNPP tracers may appear at the southern KE flank due to variations in the KE path and in the location of the meanders. This, however, does not mean that the tracers will be transported to the subtropical areas south of the KE. If a meander does not break and the KE simply retreats northward to its standard position, the tracers will be transported back to the confluence zone north of the KE, and no tracers will remain in subtropical area. Alternatively, Kuroshio rings may assist in CJT when some rings trap tracers from the northern side of the KE jet during the formation process and transport the tracers into the ring core after pinching off from the jet. In this case, the Fukushima-derived radionuclides and other tracers may end up on the southern side of the KE. Based on the multi-year statistics after the accident at the FDNPP, it has been shown that the CJT is the event when large portions of tracers coherently cross the jet during a short time interval. Comparison with the variations of the KE path shows that more efficient CJT occurred in the years of stronger meandering of the KE.

The ring-assisted mechanism has been studied in detail using altimetry-derived Lagrangian maps, the GLORYS12V1 reanalysis data, and shipboard CTD measurements. In 2024, the FDNPP virtual tracers were observed inside two cold-core rings, E and W, on the southern side of the KE. The CTD transects across these rings, implemented by R/V *Akademik Oparin* in June 2024, proved that they contained in the surface layer colder low-salinity water of subarctic origin that differed from the surrounding subtropical water. This observation of subarctic origin water in the centers of cold-core rings confirmed the Lagrangian maps showing advection of the FDNPP virtual tracers. To examine T-S structure of the rings and to trace their changes during their evolution, we used GLORYS12V1 data.

Both rings W and E were strong dynamic features with diameters around 200–250 km. The T-S anomalies associated with the rings were traced down to the maximum depth of observations, which suggests that the rings penetrated deeper than 1000 m. Strong currents up to 20 cm/s were observed down to 600–650 m depth. Very strong currents (120–160 cm/s) in the surface layer are comparable to and even exceed the flow of KE jet. The western ring W had a stronger anomaly in T-S characteristics and currents than the eastern ring E. This is probably caused by its second contact and repeated detachment from the KE and intrusion of water from the confluence zone north of the KE resulting in advection of newer FDNPP tracers into the ring. The eastern ring E was isolated from the KE for a few months. Thus, its core water was slightly modified during its evolution. The GLORYS12V1-based thermohaline vertical structure of the rings was similar to the CTD measurements. This double checking may be considered as the evidence of the subarctic origin of the core water, and it allows us to examine the T-S structure evolution of the rings. The data show slow dissipation of the rings after their separation from the KE and an increase in their strength after a second contact with the KE.

The observed cold-core rings are similar to strong cold-core rings of Kuroshio observed in this area in previous studies. Thus, we may expect that CJT caused by cold-core rings is typical phenomenon for this area. Strong rings produced by the 1st meander provide fast CJT and transport of FDNPP tracers across the KE within a few days, as observed in our tracer experiment. Longer transport could be provided by the rings formed at the 2nd meander. By contacting the KE, merging, and detaching again, the rings provide multiple events of CJT. Thus, we were able to combine long-term numerical particle tracking and the real-time detection of transient mesoscale features with targeted shipboard

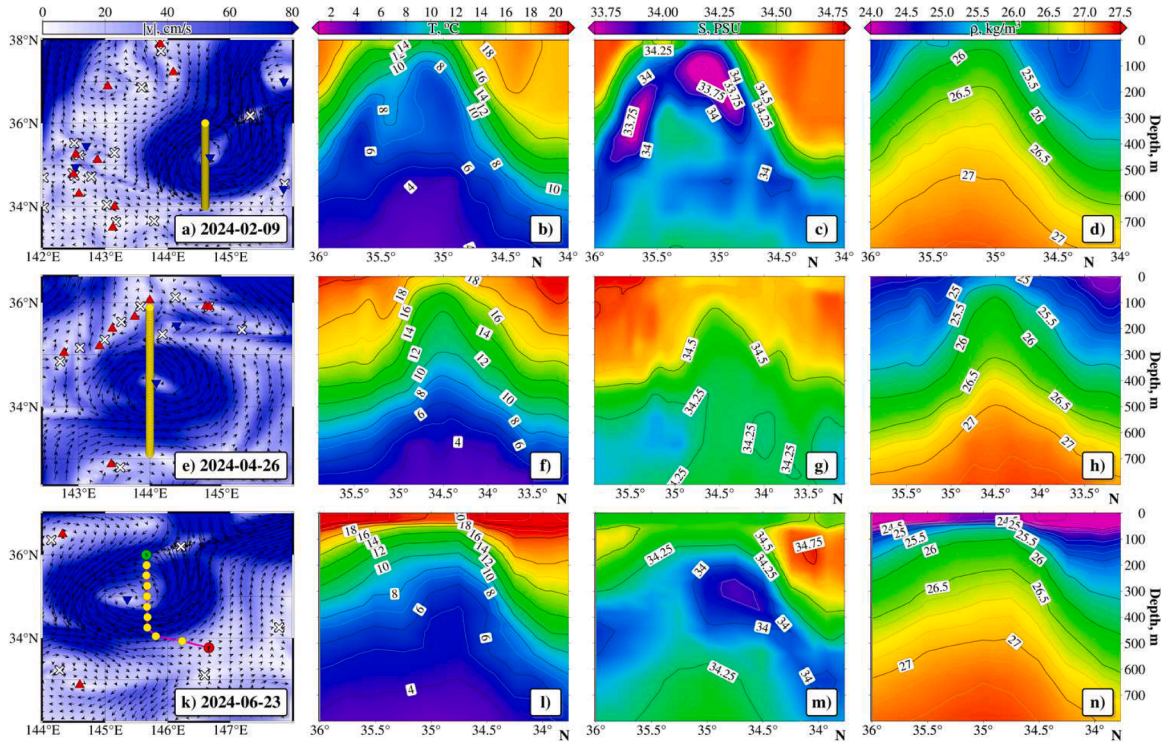


Fig. 15. Evolution of thermohaline structure of cold-core ring W based on GLORYS12V1 data for February 9 (upper panel), April 26 (middle panel) and June 23 (lower panel), 2024. (a, e, k) surface velocity field, vertical sections of (b, f, l) temperature, (c, g, m) salinity and (d, h, n) density anomaly. Location of section is shown by yellow line, CTD stations – by yellow dots. Green and red full circles are the beginning and end points of the transect. The up (down) oriented red (blue) triangles denote the elliptic points corresponding to locations of the centers of anticyclones (cyclones). Crosses are hyperbolic points.

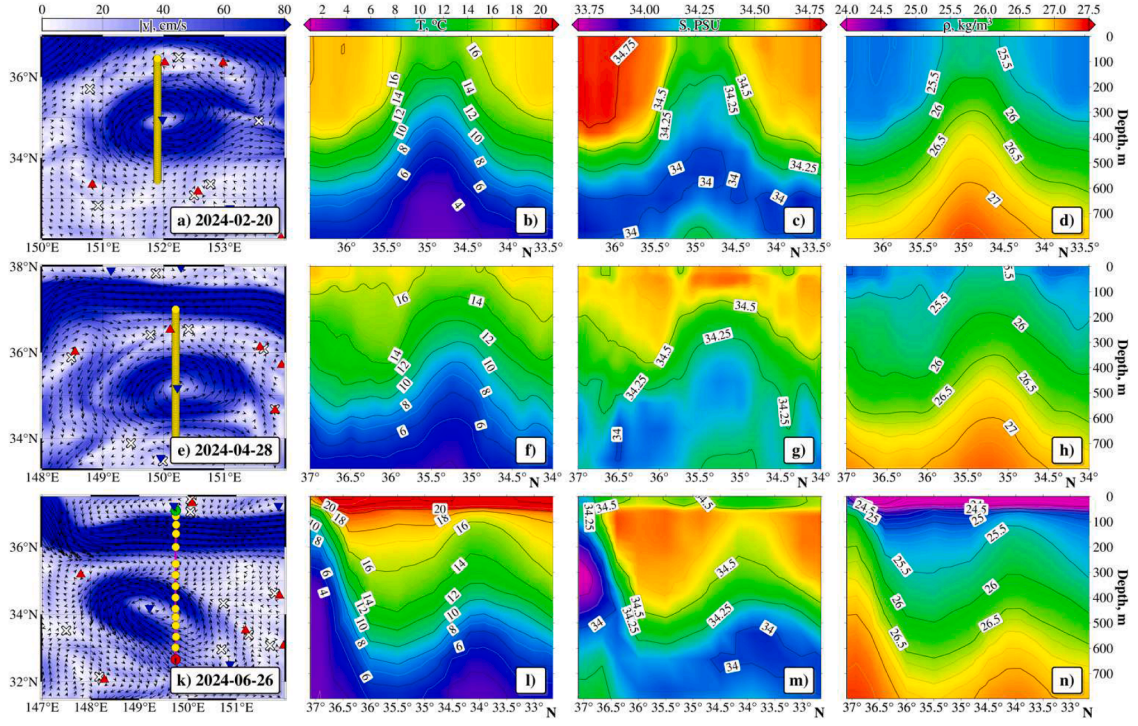


Fig. 16. Evolution of thermohaline structure of cold-core ring E based on GLORYS12V1 data for February 20 (upper panel), April 28 (middle panel) and June 26 (lower panel), 2024. (a, e, k) Surface velocity field, vertical sections of (b, f, l) temperature, (c, g, m) salinity and (d, h, n) density anomaly. Location of section is shown by yellow line, CTD stations – by yellow dots. The up (down) oriented red (blue) triangles denote the elliptic points corresponding to locations of the centers of anticyclones (cyclones). Crosses are hyperbolic points.

observations.

CRediT authorship contribution statement

M.A. Lebedeva: Visualization, Formal analysis. **M.V. Budyansky:** Validation, Investigation, Funding acquisition, Formal analysis, Data curation. **S.V. Prants:** Writing – review & editing, Writing – original draft, Supervision, Project administration, Funding acquisition, Conceptualization. **V.B. Lobanov:** Writing – review & editing, Writing – original draft, Funding acquisition, Data curation. **A.F. Sergeev:** Data curation. **A.A. Udalov:** Visualization, Investigation. **A.A. Didov:** Visualization.

Declaration of competing interest

The authors declare that they have no known competing financial interests or personal relationships that could have appeared to influence the work reported in this paper.

Acknowledgements

The work of SVP and AAU was supported by the POI project No. 124022100072-5. The work of VBL and AFS was supported by POI project No. 124022100079-4. The work of MAL, MVB and AAD was supported by St. Petersburg State University project no. 116442164. This research was conducted within the framework of the Engineering Center for Technologies of World Ocean Resources Research and Development at the POI. The ship time was provided by the Ministry of Science and Higher Education of Russian Federation. The authors are thankful to captain Mr. Igor Belousov, CTD group and the crew of R/V *Akademik Oparin* for hard work even in gale weather conditions.

Supplementary materials

Supplementary material associated with this article can be found, in the online version, at doi:10.1016/j.ocemod.2026.102814.

Data availability

The data that has been used is confidential.

References

Abdalla, S., Abdeh Kolahchi, A., Adusumilli, S., Prants, S.V., et al., 2021. Altimetry for the future: Building on 25 years of progress. Adv. Space Res. 68, 319–363. https://doi.org/10.1016/j.asr.2021.01.022.

Aoyama, M., Hamajima, Y., Hult, M., et al., 2016. 134Cs and 137Cs in the North Pacific Ocean derived from the March 2011 TEPCO Fukushima Dai-ichi nuclear power plant accident, Japan. Part one: surface pathway and vertical distributions. J. Oceanogr. 72, 53–65. https://doi.org/10.1007/s10872-015-0335-z.

Bower, A.S., Rossby, H.T., Lillibridge, J.L., 1985. The Gulf Stream – Barrier or blender? J. Phys. Oceanogr. 15 (1), 24–32.

Bower, A.S., Rossby, T., 1989. Evidence of cross-frontal exchange processes in the Gulf Stream based on isopycnal RAFOS float data. J. Phys. Oceanogr. 19 (9), 1177–1190.

Budyansky, M.V., Goryachev, V.A., Kaplunenko, D.D., et al., 2015. Role of mesoscale eddies in transport of Fukushima-derived cesium isotopes in the ocean. Deep-Sea Res. Pt. I 96, 15–27. https://doi.org/10.1016/j.dsr.2014.09.007.

Budyansky, M.V., Uleysky, M.Y., Prants, S.V., 2009. Detection of barriers to cross-jet Lagrangian transport and its destruction in a meandering flow. Phys. Rev. E 79, 056215. https://doi.org/10.1103/PhysRevE.79.056215.

Buesseler, K.O., Jayne, S.R., Fisher, N.S., 2012. Fukushima-derived radionuclides in the ocean and biota off Japan. P. Natl. Acad. Sci. USA 109, 5984–5988. https://doi.org/10.1073/pnas.1120794109.

Cedarholm, E.R., Rypina, I.I., Macdonald, A.M., Yoshida, S., 2019. Investigating subsurface pathways of Fukushima cesium in the northwest Pacific. Geophys. Res. Lett. 46, 6821–6829. https://doi.org/10.1029/2019GL082500.

Cheney, R.E., Richardson, P.L., Nagasaka, K., 1980. Tracking a Kuroshio cold ring with a free-drifting surface buoy. Deep-Sea Res. 27A 641–654.

de Verdière, A.C., Ollitrault, M., 2016. A direct determination of the world ocean barotropic circulation. J. Phys. Oceanogr. 46, 255–273. https://doi.org/10.1175/JPO-D-15-0046.1.

Flierl, G.G.R., 1981. Particle motions in large-amplitude wave fields. Geophys. Astrophys. Fluid Dyn. 18 (1–2), 39–74. https://doi.org/10.1080/03091928108208773.

Hirata, H., Nishikawa, H., Usui, N., Miyama, T., Sugimoto, S., Kusaka, A., Seto, T., 2025. The Kuroshio large meander and its various impacts: a review. J. Oceanogr. 81, 165–185. https://doi.org/10.1007/s10872-025-00753-z.

Ikenoue, T., Kawamura, H., Kamidaira, Y., 2023. Statistical analysis of simulated oceanic dispersion of dissolved radionuclide hypothetically released from the Fukushima Dai-ichi Nuclear Power Plant using long-term oceanographic reanalysis data. J. Nucl. Sci. Technol. 60 (1), 61–71. https://doi.org/10.1080/00223131.2022.2079569.

Itoh, S., Yasuda, I., 2010. Characteristics of mesoscale eddies in the Kuroshio-Oyashio Extension region detected from the distribution of the sea surface height anomaly. J. Phys. Oceanogr. 40, 1018–1034. https://doi.org/10.1175/2009JPO4265.1.

Jayne, S.R., Hogg, N.G., Waterman, S., et al., 2009. The Kuroshio Extension and its recirculation gyres. Deep-Sea Res. Pt. I 56 (12), 2088–2099. https://doi.org/10.1016/j.dsr.2009.08.006.

Kaeriyama, H., 2016. Oceanic dispersion of Fukushima-derived radioactive cesium: a review. Fish. Oceanogr. 26 (2), 99–113. https://doi.org/10.1111/fog.12177.

Kaeriyama, H., Ambe, D., Shimizu, Y., et al., 2013. Direct observation of 134Cs and 137Cs in surface seawater in the western and central North Pacific after the Fukushima Dai-ichi nuclear power plant accident. Biogeosciences 10, 4287–4295. https://doi.org/10.5194/bg-10-4287-2013.

Kaeriyama, H., Shimizu, Y., Ambe, D., et al., 2014. Southwest intrusion of 134Cs and 137Cs derived from the Fukushima Dai-ichi nuclear power plant accident in the western North Pacific. Environ. Sci. Technol. 48, 3120–3127. https://doi.org/10.1021/es403686v.

Kawai, H., 1972. Hydrography of the Kuroshio Extension. In: Stommel, H., Yoshida, K. (Eds.), Kuroshio: Its Physical Aspects. University of Tokyo Press, Tokyo, pp. 235–352.

Kawai, H., 1980. Rings south of the Kuroshio and their possible roles in transport of the intermediate salinity minimum and in formation of the skipjack and albacore fishing grounds. In: The Kuroshio IV: Proc. 4th CSK Symp., Tokyo, Japan, Feb. 1979. Saikon Publ., pp. 250–273

Kim, S.-Y., Lee, H.J., Jung, K.T., Kim, H., Kim, K.O., 2024. A study on the pathways and their interannual variability of the Fukushima-derived tracers in the northwestern Pacific. Front. Mar. Sci. 11, 1358032. https://doi.org/10.3389/fmars.2024.1358032.

Kitano, K., 1975. Some properties of the warm eddies generated in the confluence zone of the Kuroshio and Oyashio currents. J. Phys. Oceanogr. 5, 245–352.

Koshlyakov, M.N., 1986. Eddies of western boundary currents. In: Kamenkovich, V.M., Koshlyakov, M.N., Monin, A.S. (Eds.), Synoptic Eddies in the Ocean. D. Reidel, Norwell, MA, pp. 208–376.

Kumamoto, Y., 2016. Spreading of Fukushima-derived radiocesium in the western North Pacific Ocean by the end of 2014. Bunseki Kagaku 66 (3), 137–148. https://doi.org/10.2116/bunsekikagaku.66.137.

Kumamoto, Y., Aoyama, M., Hamajima, Y., Aono, T., Kouketsu, S., Murata, A., Kawano, T., 2014. Southward spreading of the Fukushima-derived radiocesium across the Kuroshio Extension in the North Pacific. Sci. Rep. 4, 4276. https://doi.org/10.1038/srep04276.

Kumamoto, Y., Murata, A., Kawano, T., Aoyama, M., 2013. Fukushima-derived radiocesium in the northwestern Pacific Ocean in February 2012. Appl. Radiat. Isotopes 81, 335–339. https://doi.org/10.1016/j.apradiso.2013.03.085.

Le Vu, B., Stegner, A., Arsouze, T., 2018. Angular momentum eddy detection and tracking algorithm (ameda) and its application to coastal eddy formation. J. Atmos. Ocean. Tech. 35 (4), 739–762. https://doi.org/10.1175/JTECH-D-17-0010.1.

Liu, Y., Hu, Z.-Z., Richmond, R.H., Zhang, J.-M., Zhao, C., Chen, S., 2026. Three-dimensional spatiotemporal simulation of tritium discharge from Fukushima. Ocean Model. 199, 102652. https://doi.org/10.1016/j.ocemod.2025.102652.

Liu, Y., Wilson, C., Green, M.A., Hughes, C.W., 2018. Gulf Stream transport and mixing processes via coherent structure dynamics. J. Geophys. Res.-Oceans 123, 3014–3037. https://doi.org/10.1002/2017JC013390.

Maderich, V., Tsumune, D., Bezhenar, R., de With, G., 2024. A critical review and update of modelling of treated water discharging from Fukushima Daiichi NPP. Mar. Pollut. Bull. 198, 115901. https://doi.org/10.1016/j.marpolbul.2023.115901.

Masuzawa, J., 1957. An example of cold eddies south of the Kuroshio. Rec. Oceanogr. Works Jpn. 3 (1), 1–7.

Mizuno, K., White, W.B., 1983. Annual and interannual variability in the Kuroshio Current system. J. Phys. Oceanogr. 13, 1847–1867.

Nakajima, R., Nagano, A., Osafune, S., Tsuchiya, M., Fujikura, K., 2024. Aggregation and transport of microplastics by a cold-core ring in the southern recirculation of the Kuroshio Extension: the role of mesoscale eddies on plastic debris distribution. Ocean Dynam 74, 773–782. https://doi.org/10.1007/s10236-024-01635-6.

Niiler, P.P., Maximenko, N.A., Panteleev, G.G., Yamagata, T., Olson, D.B., 2003. Near-surface dynamical structure of the Kuroshio Extension. J. Geophys. Res. 108, 3193. https://doi.org/10.1029/2002JC001461.

Ponomarev, V.I., Fayman, P.A., Prants, S.V., et al., 2018. Simulation of mesoscale circulation in the Tatar Strait of the Japan Sea. Ocean Model 126, 43–55. https://doi.org/10.1016/j.ocemod.2018.04.006.

Prants, S., 2023. Transport barriers in geophysical flows: a review. Symmetry 15, 1942. https://doi.org/10.3390/sym15101942.

Prants, S.V., 2021. Trench eddies in the Northwest Pacific: an overview. Izv. Atmos. Ocean. Phys. 57 (4), 341–353. https://doi.org/10.1134/S0001433821040216.

Prants, S.V., Budyansky, M.V., Uleysky, M.Yu., 2014. Lagrangian study of surface transport in the Kuroshio Extension area based on simulation of propagation of Fukushima-derived radionuclides. Nonlin. Processes Geophys. 21, 279–289. https://doi.org/10.5194/npg-21-279-2014.

Prants, S.V., 2025. Dynamical systems theory approach in oceanography: a review on achievements, limitations, verification and validation of Lagrangian methods. Front. Mar. Sci. 12, 1621820. https://doi.org/10.3389/fmars.2025.1621820.

Prants, S.V., Uleysky, M.Yu., Budyansky, M.V., 2017. Lagrangian oceanography: large scale transport and mixing in the ocean. Physics of Earth and Space Environments. Springer-Verlag, Berlin. https://doi.org/10.1007/978-3-319-53022-2.

Qiu, B., 2002. The Kuroshio Extension system: its large-scale variability and role in the midlatitude ocean-atmosphere interaction. J. Oceanogr. 58, 57–75. https://doi.org/10.1023/A:1015824717293.

Qiu, B., Chen, S., 2005. Variability of the Kuroshio Extension jet, recirculation gyre and mesoscale eddies on decadal timescales. J. Phys. Oceanogr. 35, 2090–2103. https://doi.org/10.1175/JPO2807.1.

Schlitzer, R., 2023. Ocean data view. https://odv.awi.de.

Tomosada, A., 1984. A cold ring in the Kuroshio system observed in summer 1982. Bull. Tokai Reg. Fish. Res. Lab. 113, 87–114.

Udalov, A.A., Budyansky, M.V., Prants, S.V., 2024. Census and properties of mesoscale eddies in the Kuril Basin of the Okhotsk Sea. Deep-Sea Res. Pt. I 212, 104374. https://doi.org/10.1016/j.dsr.2024.104374.

Ueno, H., Barth, J.A., et al., 2023. Review of oceanic mesoscale processes in the North Pacific: physical and biogeochemical impacts. Prog. Oceanogr. 212, 102955. https://doi.org/10.1016/j.pocean.2022.102955.

Uleysky, M.Y., Budyansky, M.V., Prants, S.V., 2010a. Mechanism of destruction of transport barriers in geophysical jets with Rossby waves. Phys. Rev. E 81, 017202. https://doi.org/10.1103/PhysRevE.81.017202.

Uleysky, M.Y., Budyansky, M.V., Prants, S.V., 2010b. Chaotic transport across two-dimensional jet streams. J. Exp. Theor. Phys. 111, 1039–1049. https://doi.org/10.1134/S1063776110120174.

Xi, C., Dong, H., Ke-feng, M., Yan, L., 2018. Detailed investigation of the three-dimensional structure of a mesoscale cold eddy in the Kuroshio Extension region. J. Oper. Oceanogr. 11 (2), 87–99. https://doi.org/10.1080/1755876X.2018.1505069.

Yasuda, I., 2003. Hydrographic structure and variability in the Kuroshio-Oyashio transition area. J. Oceanogr. 59, 389–402. https://doi.org/10.1023/A:1025580313836.

Yoshida, S., Macdonald, A.M., Jayne, S.R., et al., 2015. Observed eastward progression of the Fukushima 134Cs signal across the North Pacific. Geophys. Res. Lett. 42, 7139–7147. https://doi.org/10.1002/2015GL065259.

Yoshikawa, Y., Church, J.A., Uchida, H., White, N.J., 2004. Near bottom currents and their relation to the transport in the Kuroshio Extension. Geophys. Res. Lett. 31, L16309. https://doi.org/10.1029/2004GL020068.

Zhang, T., Hou, X., Fan, Y., 2025. Marine dispersion of Fukushima-derived radiocesium in the North Pacific and its implications. Sci. China Earth Sci. 68 (2), 389–406. https://doi.org/10.1007/s11430-024-1471-5.

Zhang, Y., Afanasyev, Y.D., 2023. Quasi-permanent meanders of the Kuroshio Extension: laboratory experiments with altimetry and numerical simulations. Ocean Model. 182, 102180. https://doi.org/10.1016/j.ocemod.2023.102180.

Zhao, C., Wang, G., Zhang, M., et al., 2021. Transport and dispersion of tritium from the radioactive water of the Fukushima Daiichi nuclear plant. Mar. Pollut. Bull. 169, 112515. https://doi.org/10.1016/j.marpolbul.2021.112515.